Constraint Enforcement for Scramjet-Powered Hypersonic Vehicles with Significant Aero-Elastic-Propulsion Interactions

Don Soloway, Armando A. Rodriguez, Jeffrey J. Dickeson, Oguzhan Cifdaloz,
Jose Benavides, Srikanth Sridharan, Atul Kelkar, and Jerald M. Vogel

Abstract— In this paper, we examine the control of a scramjet-powered hypersonic vehicle with significant aero-elastic-propulsion interactions. Such vehicles are characterized by open loop unstable non-minimum phase dynamics, low frequency aero-elastic modes, significant coupling, and hard constraints (e.g. control surface deflection limits, thrust margin). Within this paper, attention is placed on maintaining acceptable closed loop performance (i.e. tracking of speed and flight path angle commands) while satisfying hard control surface deflection constraints as well as stoichiometrically normalized fuel-equivalency-ratio (FER) margin constraints. Control surface constraints are a consequence of maximum permissible aerodynamic loading. FER margin constraints are a consequence of thermal choking (i.e. unity combustor exit Mach number) and the fact that thrust loss may not be captured for FER greater than unity. Such limits are particularly important since the vehicle is open loop unstable and "saturation" can result in instability. To address these issues, one can design conservative (i.e. less aggressive or lower bandwidth) controllers that maintain operation below saturation levels for anticipated reference commands (and disturbances). Doing so, however, unnecessarily sacrifices performance - particularly when small reference commands are issued. Within this paper, the above issues are addressed using generalized predictive control (GPC). A 3DOF longitudinal model for a generic hypersonic vehicle, which includes aero-elastic-propulsion interactions, is used to illustrate the ideas.

I. INTRODUCTION AND OVERVIEW

Motivation. Integrated airframe scramjet-powered hypersonic vehicles have recently received considerable attention because they represent the next critical step toward achieving low-cost-to-orbit and global reach vehicles. Such vehicles are often characterized by unstable non-minimum phase dynamics, low frequency flexible dynamics, significant aero-thermo-elastic-propulsion interactions, multivariable coupling, and uncertainty

This paper addresses relevant control challenges and tradeoffs associated with the enforcement of operational constraints; e.g. FER, elevator.

Modeling and Control Challenges. Modeling and control challenges associated with scramjet-powered hypersonic vehicles are discussed in [1]. The following describes control-relevant hypersonic vehicle models addressing aero-thermo-elastic-propulsion effects [2–9]. The long lower forebody of typical hypersonic waveriders combined with a rearward shifted center-of-gravity (CG), results in a pitch-up instability. The non-minimum phase (inverse response) behavior is associated with the elevator to flight-path-angle (FPA) map and is characteristic of tail-controlled vehicles [4]. While the instability requires a minimum BW for stability [10] (achievable, for example, via feedback of attitude and rate [1]), the right half plane (RHP) zero and the uncertain flexible modes limit the maximum achievable BW. State-dependent margins can limit the speed/size of the commands that may be followed. These margins can be associated with FER limits, thermal choking, and/or reduced engine performance. Thermal choking occurs when the combustor exit Mach slows down to unity - typically because of excess FER (i.e. heat addition across the combustor). Another margin (which we consider in this paper) can be due to an $FER \leq 1$ constraint that we may wish to enforce because thrust decreases due to $FER > 1$ [4]. This paper examines the importance of these margins and a method for enforcing the associated constraints. To do so, the paper exploits the modeling work discussed within [2, 3, 5, 11, 12].
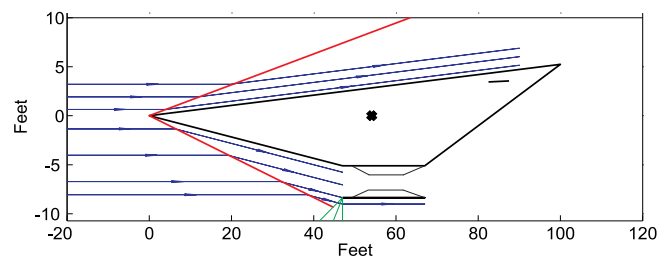

Fig. 1. Schematic of Scramjet-Powered Hypersonic Vehicle

Goals and Contributions of Paper. The purpose of this paper is to show (1) the importance of FER margins, (2) how FER margins can be computed (off-line) to obtain a static nonlinear state-dependent "saturation" map that is useful for limiting FER (on-line), (3) how FER margins depend on the flight condition (altitude, Mach, flow turn angle), and (4) how to design a control system with FER and elevator constraint enforcement built-in. Generalized predictive control (GPC) [13] was used to accomplish the

latter because it can readily accommodate state and control constraints. Items (1)-(4) have received little attention in the controls literature. Within [12], the authors address anti-windup issues for a hypersonic vehicle - specifically addressing constant (static) constraints associated with control surface deflection, total temperature across the combustor, and diffuser area ratio. To our knowledge, control systems that account for the nonlinear FER state-dependent "saturation" considered in this paper have not been addressed elsewhere.

II. DESCRIPTION OF NONLINEAR MODEL

In this paper, we consider a first principles nonlinear 3-DOF (plus flexing) model for the longitudinal dynamics of a generic scramjet-powered hypersonic vehicle [1, 2, 4–6, 11, 12, 14]. The vehicle is 100 ft long with weight (density) 6154 lb per foot of depth and has a first bending mode frequency at about 18 rad/sec. The vehicle may be visualized as shown in Figure 1 [11].

Modeling Approach. The following summarizes the modeling approach used.

Aerodynamics. Pressure distributions are computed using inviscid compressible oblique-shock and Prandtl-Meyer expansion theory [2, 15, 16]. Viscous drag effects (i.e. an analytical skin friction model) are captured using Eckerts temperature reference method [11, 15]. This relies on using the incompressible turbulent skin friction coefficient formula for a flat plate. Unsteady effects (e.g. due to rotation and flexing) are captured using linear piston theory [11, 17].

Structural. A single free-free Euler-Bernoulli beam model is used to capture vehicle elasticity. The assumed modes method is used to obtain natural frequencies, mode shapes, and finite-dimensional approximants [2]. This results in a model whereby the rigid body dynamics influence the flexible dynamics through generalized forces. Fore and aftbody deflections influence the rigid body dynamics; the former via the bow shock which influences engine inlet conditions, thrust, lift, drag, and moment [2]; the latter via the angle-of-attack (AOA) seen by the elevator.

Actuator Dynamics. Simple first order actuator models (contained within the original model) were used in each of the control channels: $A_{fer} = \frac{10}{s+10}$ for FER, $A_{ele} = \frac{20}{s+20}$ for elevator. Elevator saturation levels of $30°$ and $-15°$ were used. A state-dependent saturation level - associated with FER (e.g. thermal choking and unity FER) - was directly addressed (see discussion below). A minimum FER saturation level of 0.1 was also used.

Longitudinal Dynamics. Over the trimmable region (see Figure 2), the vehicle exhibits unstable non-minimum phase dynamics with nonlinear aero-elastic-propulsion coupling and critical (state-dependent) FER constraints [1]. The model contains 11 states: 5 rigid body states (velocity, FPA, altitude, pitch rate, pitch angle) and 6 flexible states. The equations of motion for the 3DOF flexible vehicle are given in [1, 2, 14]. The vehicle has two (2) control inputs (that
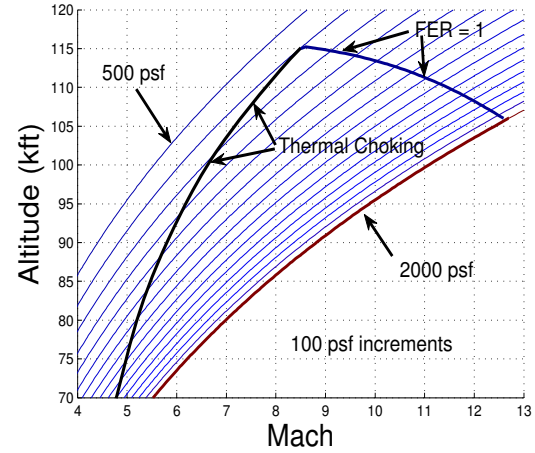

Fig. 2. Air-Breathing Corridor Illustrating Constant Dynamic Pressure Profiles, Thermal Choking and FER Barriers; Notes: (1) Vehicle considered in this paper cannot be trimmed above thermal choking line; (2) An FER ≤ 1 constraint is enforced to stay within validity of model; (3) Constraints obtained using viscous-unsteady model for level flight [2, 4–6, 11, 12, 14]

will be used in this paper): a rearward situated elevator δ_e and stoichiometrically normalized fuel equivalence ratio (FER). Relevant propulsion model components are discussed below. Additional details about the model may be found within the following references [2, 4–6, 11, 12, 14, 18]. Limitations of the model are addressed within [1, 19].

III. ANALYSIS OF SCRAMJET

Trimmable Region (Level-Flight). Figure 2 shows the altitude-Mach range over which the vehicle can be trimmed in level-flight. Thermal choking, $FER = 1$, and $\bar{q} = 2000$ psf dynamic pressure barriers are shown.

Scramjet Model. The scramjet engine model is that used in [2, 3]. It consists of an inlet, an isentropic diffuser, a 1D Rayleigh flow combustor (frictionless duct with heat addition [16]), and an isentropic internal nozzle. A single (long) forebody compression ramp provides conditions to the rear-shifted scramjet inlet. Although the model supports a variable geometry inlet, we will not be exploiting variable geometry in this paper; i.e. diffuser area ratio $A_d \stackrel{\text{def}}{=} \frac{A_2}{A_1}$ will be fixed with $A_d = 1$, see Figure 3).
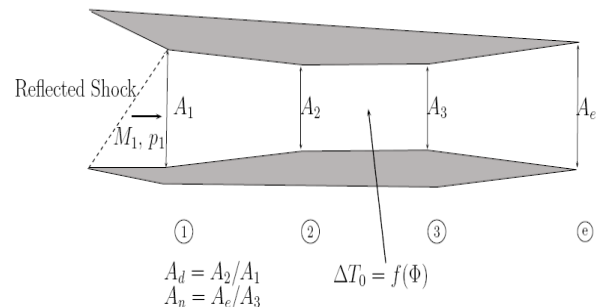

Fig. 3. Schematic of Scramjet Engine

Translating Cowl Door. The model assumes the presence of an (infinitely fast) translating cowl door which uses AOA to achieve shock-on-lip conditions (assuming no forebody flexing). Forebody flexing, however, results in an oscillatory bow shock and air mass flow spillage [2]. A bow shock reflection (off of the cowl or inside the inlet) further slows down the flow and steers it into the engine. Shock-shock interactions are not modeled.

Combustor Entrance Properties. The combustor entrance properties are found using the formulae in [1, 2], [16, pp. 103-104]: $M_2 = M_2(M_1, A_d, \gamma)$, $T_2 = T_2(M_1, M_2, A_d, \gamma)$, $p_2 = p_2(M_1, M_2, A_d, \gamma)$ where $A_d \overset{\text{def}}{=} \frac{A_2}{A_1}$ is the diffuser area ratio.

Combustor Exit Properties. The model uses liquid hydrogen (LH2) as the fuel. If f denotes fuel-to-air ratio and f_{st} denotes stoichiometric fuel-to-air ratio, then the stoichiometrically normalized fuel equivalency ratio is given by $FER \overset{\text{def}}{=} \frac{f}{f_{st}}$ [20], [2]. FER is the engine control. The combustor exit properties can be determined using the formulae in [1, 2], [16, pp. 103-104]. First, one computes the change in total temperature across the combustor: $\Delta T_c = \Delta T_c(T_{t_2}, FER, H_f, \eta_c, c_p, f_{st}) = \left[\frac{f_{st} FER}{1 + f_{st} FER}\right]\left(\frac{H_f \eta_c}{c_p} - T_{t_2}\right)$ where $H_f = 51,500$ BTU/lbm is the heat of reaction for liquid hydrogen (LH2), $\eta_c = 0.9$ is the combustion efficiency, $c_p = 0.24$ BTU/lbm°R is the specific heat of air at constant pressure, and $f_{st} = 0.0291$ is the stoichiometric fuel-to-air ratio for LH2. One can then try to solve for $M_3 = M_3\left(M_2, \frac{\Delta T_c}{T_2}, \gamma\right)$. This will have a solution provided that M_2 is not too small, ΔT_c is not too large (FER is not too large [1]), or T_2 is not too small.

Combustor Thermal Choking FER. FER directly determines the change in total temperature across the combustor resulting from the combustion process. Once the change in total temperature across the combustor ΔT_c has been computed, one can "try" to solve for the combustor exit Mach M_3. As described within [1], a solution will exist provided that FER is not too large, T_2 is not too small (high altitudes), and the combustor entrance Mach M_2 is not too small (large flow turn angle). When $M_3 = 1$, *thermal choking* [16, 20] is said to exist at the combustor exit. The FER that produces $M_3 = 1$ is FER_{TC} and is referred to as the *thermal choking FER*. FER_{TC} is a function of the free-stream Mach M_∞, the free-stream temperature T_∞ (altitude), and the FTA (since τ_{1l} is a vehicle constant). Physically, the addition of heat to a supersonic flow causes the flow to slow down. When thermal choking occurs, it is not possible to increase the air mass flow through the engine. Propulsion engineers want to operate near thermal choking for engine efficiency reasons [20]. However, if additional heat is added, the upstream conditions can be altered and it is possible that this may lead to engine unstart. This is highly undesirable. For this reason, operating near thermal choking has been described by some propulsion engineers as "operating near the edge of a cliff."
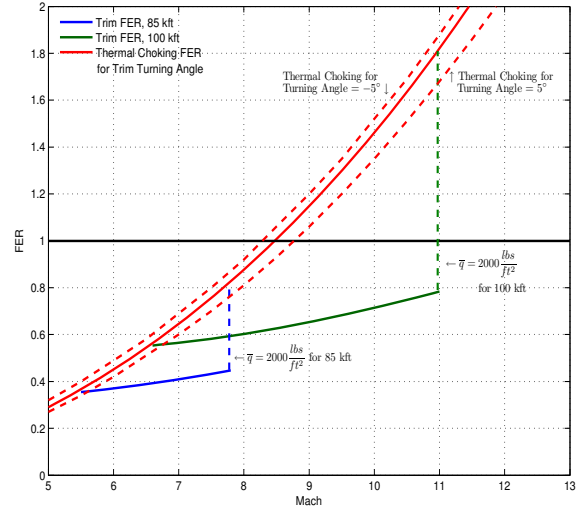

Fig. 4. Visualization of FER Margins, Trim FER vs Mach for different altitudes, FER_{TC} vs Mach for different flow turning angles (FTAs) - Level-Flight, Unsteady-Viscous Flow, 2 Controls, Flexible Vehicle

Trim FER. Within Figure 4, we can see the trim FER for level-flight at 85 kft (blue) and 100 kft (green) as Mach is varied. We observe that trim FER increases with altitude, Mach, and as we climb constant dynamic pressure profiles.

Thermal Choking FER Properties. Figure 4 demonstrates FER margin properties that are characteristic of hypersonic vehicles. Figure 4 shows FER_{TC} for $FTA \in [-5°, 5°]$ (red curves). The solid red curve corresponds to a zero FTA. The lower (upper) dashed red curve corresponds to FTA of $5°$ (-5°). Consequently, FER_{TC} depends on the FTA. To summarize, FER_{TC} is (nearly) independent of altitude (for constant FTA, not shown in figure), decreases with decreasing Mach (for constant FTA), decreases (increases) with increasing (decreasing) FTA (for constant Mach).

Thermal Choking and Unity FER Margins. Next, we define FER margins that are useful for control system design. While the patterns revealed are based on the simple 1D Rayleigh flow model discussed above, the FER margin framework introduced is useful for designing control systems that suitably tradeoff scramjet authority and efficiency.

Thermal Choking FER Margin. The *thermal choking margin* at an instant in time is defined as follows:

$$FERM_{TC} \overset{\text{def}}{=} FER_{TC} - FER. \tag{1}$$

Since FER_{TC} depends upon altitude (free-stream temperature), free-stream Mach, and the FTA (hence vehicle state), so does $FERM_{TC}$. $FERM_{TC}$ measures FER control authority (or saturation margin) at a given time instant. It also measures the scramjet's ability to accelerate the vehicle. While an accurate FTA measurement may not be available, the $FERM_{TC}$ concept - when combined with measurements, models, and uncertainty bounds - could be

very useful for controlling how close the scramjet gets to thermal choking; i.e. "to the edge of the cliff."

Trim FERM Properties. For a fixed FER, $FERM_{TC}$ exhibits behavior similar to the FER_{TC} (see above). Now suppose that FER is maintained at some trim FER and that the FTA is nearly constant; e.g. constant AOA and little flexing. For a nearly constant FTA and trim FER, $FERM_{TC_{trim\,fer}}^{FTA}$ decreases with decreasing Mach (altitude fixed), decreases with increasing altitude (Mach fixed), decreases with decreasing altitude and Mach along a constant $\bar{q}$ profile. Why is this? $FERM_{TC_{trim\,fer}}^{FTA}$ decreases with decreasing Mach because as Mach decreases, the FER_{TC} decreases faster than the trim FER; both decrease quadratically, but FER_{TC} decreases faster (Figure 4). It decreases with increasing altitude because as altitude increases, FER_{TC} remains constant while the trim FER increases. It decreases with decreasing altitude and Mach along a constant dynamic pressure profile because the trim FER decreases more slowly than FER_{TC} along such profiles. If one uses trim values, then one obtains $trim\ FERM_{TC} = \text{trim}\,FER_{TC} - \text{trim}\,FER$. Its dependence on the flight condition is more difficult to analyze since the trim FTA changes with the flight condition.

Unity FER Margin. Within the model, thrust is linearly related to FER for all expected FER values - leveling off at (unrealistically) large FER values. In practice, when $FER > 1$, the result is decreased thrust. This phenomena is not captured in the model [2]. As such, control designs based on this model (or derived linear models) should try to maintain FER below unity. This motivates the instantaneous FER unity margin:

$$FERM_{unity} \overset{\text{def}}{=} 1 - \text{FER}. \tag{2}$$

Figure 4 shows that if FER is set to a trim FER, then $FERM_{unity}^{trim\,fer}$ decreases with increasing Mach or increasing altitude because trim FER increases with Mach and altitude.

FER Margin ($FERM$). Given the above, it is reasonable to define the *instantaneous FER margin FERM* as follows:

$$FERM \overset{\text{def}}{=} \min \{ FERM_{TC}, FERM_{unity} \}. \tag{3}$$

Alternatively, $FERM \overset{\text{def}}{=} \min \{ FER_{TC}, 1 \} - FER$. It should be emphasized that at any time instant the FERM depends on the system state (i.e. M_∞, altitude via T_∞, FTA). The trim FERM also depends on p_∞. The static nonlinear FERM map has been determined for our simple Rayleigh-based model. This "saturation" map is used when applying control laws to the nonlinear model to ensure that $FER > FER_{TC}$ is never applied. This is important because the simulation "crashes" if too large an FER is issued; i.e. hypersonic vehicles have low thrust margins [21].

Limitations of Analysis. The above is based on the simple 1D Rayleigh scramjet model being used. Thermal choking, strictly speaking, is not a 1D phenomena. Given this, the

impact of 2D effects and finite-rate chemistry on estimating FERM will be examined in future work [19, 22].

IV. GENERALIZED PREDICTIVE CONTROL

In this paper, we use generalized predictive control (GPC) for FER margin and elevator saturation constraint enforcement as well as for control. The control architecture used is discussed in [13]. The objective function is a quadratic cost functional with receding finite prediction and control horizons. The GPC controller assumes access to velocity, velocity command, FPA, FPA command, pitch, and pitch rate. For prediction purposes, a linear model - including flexible states, altitude, and no actuator dynamics - was used. When saturations are included during prediction, this includes the elevator saturation levels as well as the current FER margin value. That is, we found it sufficient to use the current FER margin throughout the entire prediction cycle. For evaluation purposes, we used the linear model without and with the saturations as well as the nonlinear model.

V. SIMULATION RESULTS

Within this section, we present our main simulation results. Nominally, the vehicle is flying level at Mach 8, 85kft. Investigated command scenarios include: (1) 2000, 4000 ft/sec velocity commands, (2) $3°$, $6°$ FPA commands. While emphasis is placed on command following, a similar approach can be taken for disturbance attenuation.

Nonlinear Responses to Velocity Commands (Unconstrained). Figure 5 contains responses to 2000 and 4000 ft/s velocity commands. These include responses whereby the linear model with saturations (i.e. nonlinear FER map, 0.1 lower FER limit, and elevator saturation levels) is used for prediction and control as discussed earlier. These linear-with-saturation responses will hereafter be referred to as the lin-sat responses. It also includes responses for the full nonlinear model (also containing the aforementioned saturations). No constraint enforcement is included. Deviation between the responses is observed to increase with the size of the velocity command. As expected, when thermal choking and unity FER limits are hit, vehicle acceleration becomes limited - see ramp-like behavior in lin-sat velocity responses. The slow down (w.r.t the linear response) results in FPA, AOA, pitch, and altitude dropping unacceptably. This gets worse for larger commands. Rather than scaling back commands and/or controller bandwidth (thus sacrificing performance for small commands), we propose to use constraint enforcement.

Nonlinear Responses to Velocity Commands (Constrained). Figure 6 contains nonlinear and lin-sat responses to 2000 and 4000 ft/s velocity commands. Constraint enforcement is included. FER is observed to hit and stay at the rails - resulting in maximum acceleration.

Nonlinear Responses to FPA Commands (Unconstrained). Figure 7 shows nonlinear and lin-sat responses to $3°$, $6°$ FPA commands. No constraint enforcement is included. The figure shows good agreement for smaller FPA commands between the nonlinear and the lin-sat. For the
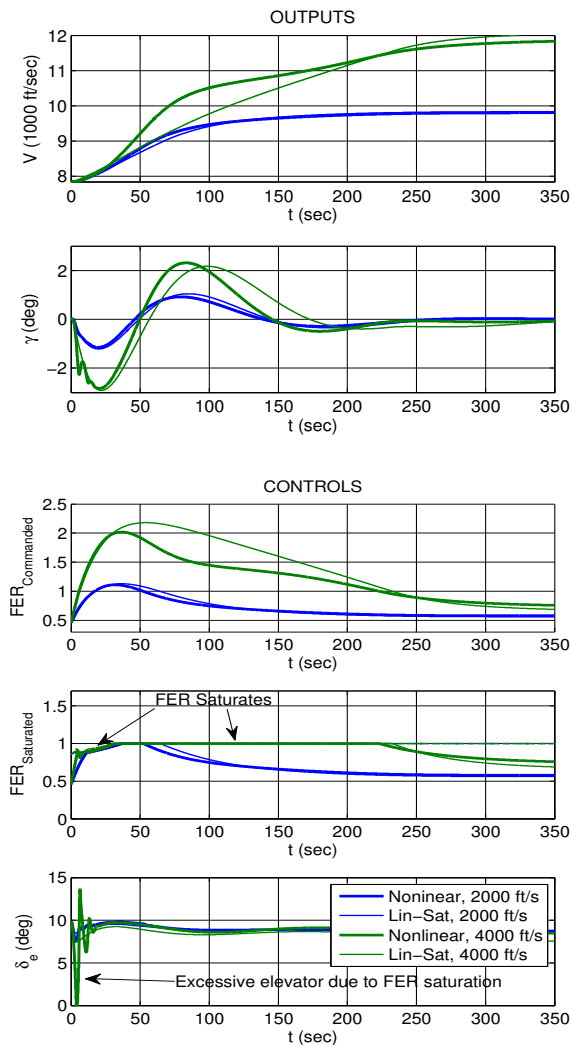
Fig. 5. Nonlinear and Lin-Sat Responses to 2000, 4000 ft/s Velocity Commands - No Constraint Enforcement
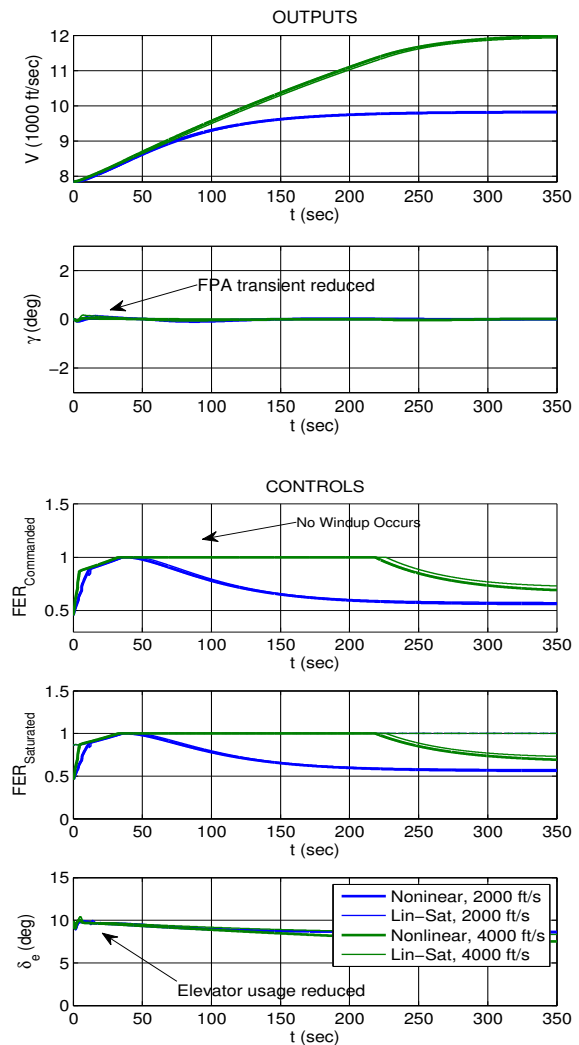

Fig. 6. Nonlinear and Lin-Sat Responses to 2000, 4000 ft/s Velocity Commands - With Constraint Enforcement

large FPA command, however, the lin-sat responses go unstable while the nonlinear responses do not go unstable. This is because the nonlinear sim exhibits no elevator saturation while the lin-sat sim does.

Nonlinear Responses to FPA Commands (Constrained). Figure 8 shows nonlinear and lin-sat responses to $3°$, $6°$ FPA commands. Constraint enforcement is included. The figure shows that adding constraint enforcement corrects the windup issues discussed earlier - keeping the controls close to the saturation rails.

VI. SUMMARY AND FUTURE DIRECTIONS

Within this paper, we have shown the importance of FER margins (e.g. thermal choking and unity) as they relate to vehicle performance and control design. While the RHP pole and zero imposes BW constraints, the FER margin constraints impose BW and reference command size constraints. GPC-based constraint enforcement was used to address thermal choking, unity FER, and elevator saturation constraint issues in a systematic non-conservative manner. Future work will examine how the FER margin map and

the shape of the trimmanble region (in Figure 2) changes when a higher fidelity model [19, 22] is used. We will also examine other constraint enforcement methods [12], [23].

REFERENCES

[1] A. Rodriguez, J. Dickeson, O. Cifdaloz, R. McCullen, J. Benavides, S. Sridharan, A. Kelkar, J. Vogel, and D. Soloway, "Modeling and Control of Scramjet-Powered Hypersonic Vehicles: Challenges, Trends, & Tradeoffs," in *AIAA GNC Conf & Exhibit, 2008-6793*, 2008.

[2] M. A. Bolender and D. B. Doman, "A Non-Linear Longitudinal Dynamical Model of an Air-Breathing Hypersonic Vehicle," *J. Spacecraft and Rockets*, vol. 44 no. 2, pp. 373 – 387, 2007.

[3] F. R. Chavez and D. K. Schmidt, "Analytical Aeropropulsive/Aeroelastic Hypersonic-Vehicle Model with Dynamic Analysis," *J. Guidance, Control and Dynamics*, pp. 1308 – 1319, 1994.

[4] M. Bolender and D. Doman, "Flight Path Angle Dynamics of Air-Breathing Hypersonic Vehicles," Airforce Research Laboratory (AFRL), Wright Patterson AFB, pp. 1 – 37, Tech. Rep., 2005.

[5] J. T. Parker, A. Serrani, S. Yurkovich, M. A. Bolender, and D. B. Doman, "Control-oriented modeling of an air-breathing hypersonic vehicle," *AIAA J. Guidance, Control, and Dynamics*, 2007.
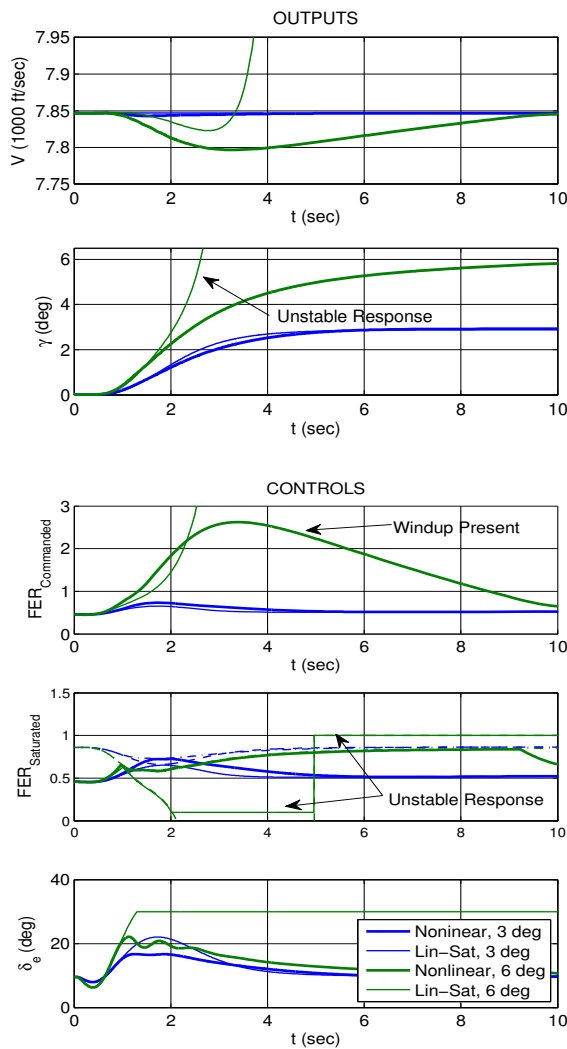
Fig. 7. Nonlinear and Lin-Sat Responses to $3°$, $6°$ FPA Commands - No Constraint Enforcement
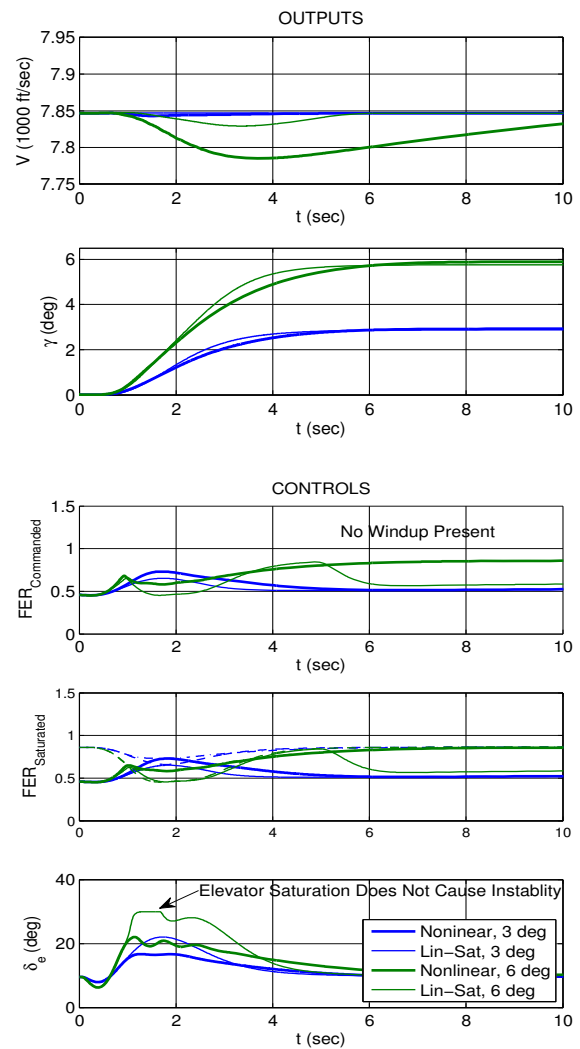

Fig. 8. Nonlinear and Lin-Sat Responses to $3°$, $6°$ FPA Commands - With Constraint Enforcement

[6] K. Groves, D. Sigthorsson, A. Serrani, S. Yurkovich, M. Bolender, and D. Doman, "Reference Command Tracking for a Linearized Model of an Air-Breathing Hypersonic Vehicle," in *AIAA Guidance, Navigation and Control Conf. and Exhibit, Paper No. 2005-6144*, 2005.

[7] E. Baumann, C. Bahm, B. Strovers, R. Beck, and M. Richard, "The X-43A Six Degree of Freedom Monte Carlo Analysis," in 46th *AIAA Aerospace Sciences Meeting and Exhibit, Paper No. 2008-203*, 2008.

[8] A. Clark, C. Wu, M. Mirmirani, and S. Choi, "Development of an Airframe Integrated Generic Hypersonic Vehicle Model," in *AIAA Aerospace Conference and Exhibit,Paper No. 2006-6560*, 2006.

[9] S. Keshmirir, "Nonlinear and Linear Longitudinal and Lateral-Directional Dynamical Model of Air-Breathing Hypersonic Vehicle," in 15th *AIAA Int Space Planes & Hypersonic Sys & Tech Conf*, 2008.

[10] G. Stein, "Respect the Unstable," IEEE Control Systems Magazine, August 2003, pp. 12 - 25.

[11] M. Bolender, M. Oppenheimer, and D. Doman, "Effects of Unsteady and Viscous Aerodynamics on the Dynamics of a Flexible Air-Breathing Hypersonic Vehicle," in *AIAA Atmospheric Flight Mechanics Conf, and Exhibit, Paper No. 2007-6397*, 2007.

[12] K. P. Groves, A. Serrani, S. Yurkovich, M. Bolender, and D. Doman, "Anti-windup control for an air-breathing hypersonic vehicle model," AFRL, Wright Patterson AFB, pp. 1 − 27, Tech. Rep., 2005.

[13] D. Soloway and P. Haley, "Pilots Rate Augmented Generalized Predictive Control for Reconfiguration," in *Proc ACC*, July, 2004.

[14] M. Bolender and D. Doman, "Modeling Unsteady Heating Effects on the Structural Dynamics of a Hypersonic Vehicle," in *AIAA Atmospheric Flight Mechanics Conf and Exhibit, 2006-6646*, 2006.

[15] J. Anderson, *Hypersonic and High-Temperature Gas Dynamics*. Sec-

ond Edition. AIAA, 2006.

[16] ——, *Modern Compress Flow, 3rd Ed*. McGraw-Hill, 2002.

[17] M. W. Oppenheimer and D. B. Doman, "A Hypersonic Vehicle Model Developed with Piston Theory," in *AIAA 2006-6637*, 2006.

[18] M. A. Bolender and D. B. Doman, "A Non-Linear Model for the Longitudinal Dynamics of a Hypersonic Air-Breathing Vehicle," in *Proceedings of the 2005 GNC Conf., 2005-6255*, 2005.

[19] S. Torrez, N. Scholten, J. Driscoll, M. Bolender, M. Oppenheimer, and D. D. Doman, "Dynamics of Hypersonic Vehicles: Shift of Poles / Zeros by Improved Propulsion Modeling ," in *AIAA Atmospheric Flight Mechanics Conf. and Exhibit, Paper No. 2008-6386*, 2008.

[20] W. H. Heiser, D. T. Pratt, D. Daley, and U. Mehta, *Hypersonic Airbreathing Propulsion*. AIAA, 1994.

[21] C. R. McClinton, J. L. Hunt, R. H. Ricketts, P. Reukau, and C. L. Peddie, "Airbreathing Hypersonic Technology Vision Vehicles and Development Dreams," in *AIAA International Space Planes and Hypersonic Systems and Technologies Conf., Paper No. 1999-4978*, 1999.

[22] R. Starkey, D. Liu, R. Chang, and P. Chem, "Rapid Conceptual Design and Analysis of a Hypersonic Air-Breathing Missile ," in 15th *AIAA Int Space Planes & Hypersonic Sys & Tech Conf, 2008-2590*, 2008.

[23] A. Teel, "Anti-Windup for Exponentially Unstable Linear Systems," *Int. J. of Robust and Nonlinear Control*, vol. 9, pp. 701–716, 1999.